LETTERS

Generating single microwave photons in a circuit

A. A. Houck[1]*, D. I. Schuster[1]*, J. M. Gambetta[1], J. A. Schreier[1], B. R. Johnson[1], J. M. Chow[1], L. Frunzio[1], J. Majer[1], M. H. Devoret[1], S. M. Girvin[1] & R. J. Schoelkopf[1]

Microwaves have widespread use in classical communication technologies, from long-distance broadcasts to short-distance signals within a computer chip. Like all forms of light, microwaves, even those guided by the wires of an integrated circuit, consist of discrete photons[1]. To enable quantum communication between distant parts of a quantum computer, the signals must also be quantum, consisting of single photons, for example. However, conventional sources can generate only classical light, not single photons. One way to realize a single-photon source[2] is to collect the fluorescence of a single atom. Early experiments measured the quantum nature of continuous radiation[3,4], and further advances allowed triggered sources of photons on demand[5–11]. To allow efficient photon collection, emitters are typically placed inside optical or microwave cavities[12–19], but these sources are difficult to employ for quantum communication on wires within an integrated circuit. Here we demonstrate an on-chip, on-demand single-photon source, where the microwave photons are injected into a wire with high efficiency and spectral purity. This is accomplished in a circuit quantum electrodynamics architecture[20], with a microwave transmission line cavity that enhances the spontaneous emission of a single superconducting qubit. When the qubit spontaneously emits, the generated photon acts as a flying qubit, transmitting the quantum information across a chip. We perform tomography of both the qubit and the emitted photons, clearly showing that both the quantum phase and amplitude are transferred during the emission. Both the average power and voltage of the photon source are characterized to verify performance of the system. This single-photon source is an important addition to a rapidly growing toolbox for quantum optics on a chip.

When an atom or qubit is strongly coupled to a cavity, the spontaneous emission rate to the output mode of the cavity is enhanced, a process known as the Purcell effect[21]. This effect has been used for a triggered single-photon source[14–16]. The underlying principle for this source is straightforward: each time the qubit is excited with a control pulse, it can emit one (and only one) photon when it decays. When the qubit is put in an arbitrary superposition state, this state is mapped onto a superposition of zero and one photon, thus transferring information from a stationary to a flying qubit. The challenge is to create a system where spontaneous emission dominates other relaxation channels. This spontaneous emission rate can be determined from the hamiltonian of the system, the well-known Jaynes–Cummings hamiltonian, $H = \hbar\omega_a\sigma_z/2 + \hbar\omega_c(a^\dagger a + 1/2) + \hbar g(a^\dagger\sigma_- + a\sigma_+)$. The first two terms represent a qubit with frequency ω_a described by Pauli operators σ_x, σ_y and σ_z, and raising and lowering operators σ_+ and σ_-, and a single cavity mode of frequency ω_c described by the photon creation and annihilation operators $a^\dagger$ and a. The final term represents a coupling of strength g between the qubit and the photon, which mixes the individual qubit and photon eigenstates. When far detuned ($\Delta = \omega_c - \omega_a \gg g$), the qubit acquires a small photonic component of the wavefunction, of magnitude g/Δ. This opens up a new source of decay for the qubit, as the photonic component of the qubit can emit at the cavity decay rate κ, resulting in a new qubit decay rate $\gamma_\kappa = (g/\Delta)^2\kappa$. The qubit can be an efficient photon source if this new decay rate dominates over other non-radiative decay rates, $\gamma_\kappa > \gamma_{NR}$.

Verifying the single-photon output is a substantial challenge in on-chip microwave experiments. The simplest approach, that of looking for a photon each time one is created, is not currently possible; unlike in optical frequency experiments, no detectors can yet resolve single-microwave photon events in a single shot. Fortunately, several unique characteristics of the source are evident in the average signal generated by many single-photon events, together yielding a convincing verification even with noisy detectors. First, the output of the single-photon source is expected to be oscillatory in the amplitude of the control pulse applied to rotate the qubit. Second, the average amplitude produced should agree well with the expected value for a single photon. Third, and most importantly, if the output of the system depends only on the state of the qubit, state tomography measured for the photons should show complete agreement with that obtained from independent measurements of the qubit. The source reported here meets all three of these criteria.

The source is implemented in a circuit quantum electrodynamics system consisting of a superconducting transmon qubit[22], an optimized version of the 'Cooper pair box'[23], capacitively coupled to a half-wave transmission line cavity with fundamental frequency $\omega_c/2\pi = 5.19$ GHz (see Fig. 1). Two important design differences between this circuit and previous incarnations of circuit quantum electrodynamics[1,24] are needed to achieve efficient single-photon generation. First, the cavity is asymmetric in that the capacitors (mirrors) at either end of the transmission line are no longer identical, resulting in asymmetric decay rates to the input and output ports ($\kappa_{in}/2\pi \approx 200$ kHz for the input side and $\kappa_{out}/2\pi = 44$ MHz for the output). As a result, photons generated in the cavity are emitted at the output port more than 99% of the time. In addition, the total decay rate for the cavity, $\kappa/2\pi = 44$ MHz, is substantially higher than in previous samples, a necessary change for spontaneous emission to be the dominant relaxation channel for the qubit. The qubit decay rate in the absence of spontaneous emission, γ_{NR}, is frequency-dependent, with $\gamma_{NR}/2\pi < 2$ MHz for all measured transmission frequencies between 4.3 and 7.3 GHz.

Transmission measurements are used to probe the energy spectrum of this system while the qubit frequency is tuned via an external magnetic field (see Fig. 2). When the qubit is far detuned from the cavity, only a single transmission peak is observed, centred at the cavity frequency with a lorentzian line shape and linewidth given by the bare cavity width. When the qubit and cavity are resonant, two peaks in transmission are seen, a phenomenon known as the vacuum Rabi splitting. Each peak corresponds to one of the two single-excitation eigenstates of the system, which are superpositions of the separate qubit and photon excitation states. The width of each

[1]Departments of Applied Physics and Physics, Yale University, New Haven, Connecticut 06520, USA.
*These authors contributed equally to this work.

peak is the average of the qubit and photon decay rates, $(\gamma + \kappa)/2$. In the dispersive limit, where the detuning Δ is much larger than the coupling g, spontaneous emission is enhanced by the Purcell effect[21], resulting in approximate decay rates $[1 - (g/\Delta)^2]\kappa + (g/\Delta)^2\gamma$ of the cavity and $[1 - (g/\Delta)^2]\gamma + (g/\Delta)^2\kappa$ of the qubit. The experimentally determined linewidths agree well with theoretical predictions (Fig. 2b), demonstrating our ability to tune the rate of radiative decay of the qubit by tuning its frequency.

It is this enhanced qubit decay due to the cavity that is used in generating single photons: the qubit line broadens when the decay of the photon-like part of the wavefunction dominates the non-radiative qubit decay. For the results presented here, the qubit was tuned to a frequency $\omega_a/2\pi = 4.68$ GHz. With a coupling $g/2\pi = 107$ MHz, the qubit wavefunctions had a $(g/\Delta)^2 = 4\%$ photonic nature, resulting in a spontaneous emission rate $\gamma_\kappa/2\pi = 1.9$ MHz. The measured relaxation rate of the qubit was $\gamma/2\pi = 1.8 \pm 0.1$ MHz, indicating that the observed relaxation could be mostly accounted for by spontaneous emission to the output transmission line to within our measurement accuracy. Because the lifetime of the qubit is short, the photon source is effectively reset in under 1 μs, allowing for rapid repeated photon generation, for a peak source power of 3 aW.

To verify single-photon generation, we first show that the output of the cavity is an oscillatory function of the input drive, as at most one photon is generated, regardless of the magnitude of the input drive. A 12 ns gaussian control pulse rotates the qubit state by a Rabi angle that is proportional to the pulse amplitude. The excited qubit will then relax, generating a new photon state at the qubit frequency (Fig. 3 inset). Because the control pulse leaves the cavity at a rate that is much faster than the rate of spontaneous emission, γ_κ, the control pulse and generated photons can easily be separated in time. As seen in Fig. 3a, the measured control signal increases monotonically, while the spontaneous emission oscillates as the qubit is rotated from the ground to the excited state and back, confirming that the spontaneous emission is proportional to the qubit state, not simply to the applied drive amplitude. This is the key to the experiment: a superposition of many photons incoming on one temporal mode give rise to one (and only one) photon on a distinct outgoing temporal mode. Moreover, because a single photon is the maximum output, the source is insensitive (to first-order) to fluctuations in the control pulse when generating one photon.

We characterize both the power and electric field of the single-photon source, using independent measurements of the qubit state made with dispersive readout techniques[25] to verify performance (Fig. 3). If the qubit state is mapped to the photon state, then an arbitrary superposition of the ground and excited states $\alpha|g\rangle + \beta|e\rangle$ will result in the same superposition of photon states: $\alpha|0\rangle + \beta|1\rangle$, where $|0\rangle$ and $|1\rangle$ refer to states with zero or one photon. The average photon number is proportional to the average qubit excitation probability, $\langle a^\dagger a\rangle = (\langle\sigma_z\rangle + 1)/2$, and has a maximum of one photon when the qubit is in the purely excited state. The two quadratures of homodyne voltage, on the other hand, are proportional to the x and y components of the qubit state: $\langle a + a^\dagger\rangle = \langle\sigma_x\rangle$ and $i\langle a^\dagger - a\rangle = \langle\sigma_y\rangle$. The measured homodyne voltage is therefore a $\pi/2$ rotation out-of-phase with the measured power, and the homodyne voltage is zero when a single photon is generated, because there is complete phase uncertainty in a photon Fock state.

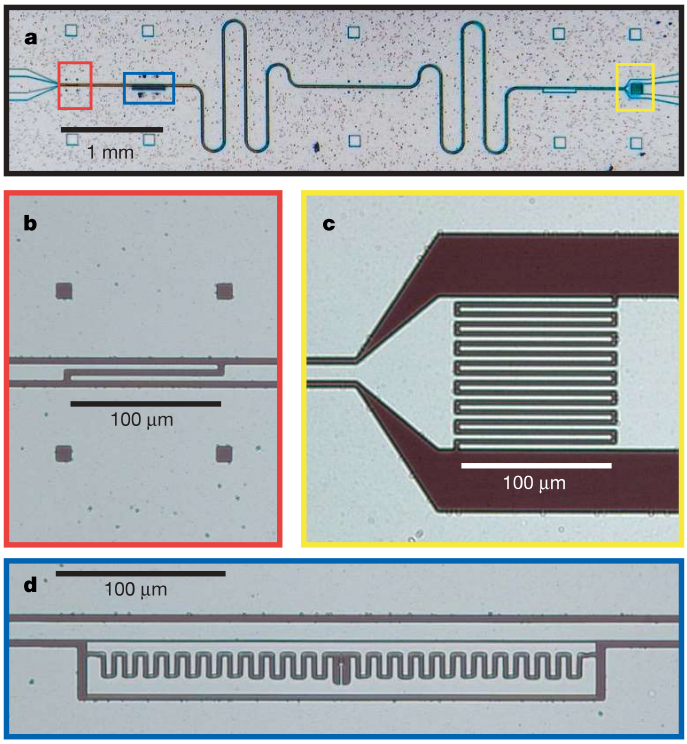

Figure 1 | The circuit quantum electrodynamics device for generating single photons. **a**, A transmission line cavity (180 nm Al on a SiO_2/Si substrate) is formed between two capacitors, with the input capacitor shown in **b** (red box in **a**) and the output in **c** (yellow box in **a**). Because the output capacitor is much larger, most radiation leaving the cavity leaves from this port, allowing efficient collection of light emitted from the cavity. **d**, Transmon qubit (100-nm-thick aluminium), an optimized 'Cooper pair box', at a voltage anti-node of the cavity (blue box in **a**). The qubit is characterized by a Josephson energy, tuned by an applied magnetic field with a maximum of $E_J^{max}/h = 20.2$ GHz and a charging energy $E_c/h = 0.37$ GHz. The coupling to the cavity is $g/2\pi = 107$ MHz at the qubit frequency primarily used in this paper, $\omega_a/2\pi = 4.68$ GHz, and has a slight dependence on the qubit frequency. The transition from the first to second excited state, $\omega_{12}/2\pi = 4.19$ GHz, is sufficiently different from ω_a to treat the qubit as a two-level system.

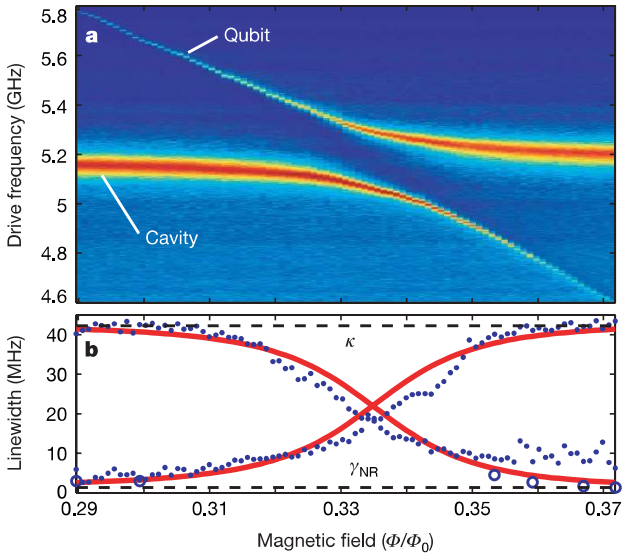

Figure 2 | Enhanced spontaneous emission through the Purcell effect. **a**, Transmission through the cavity–qubit system at different applied fluxes (log scale). Two peaks are evident in transmission due to the vacuum Rabi splitting. Away from the avoided crossing, these peaks correspond to 'mostly qubit' and 'mostly cavity' states. The bare linewidth of the cavity, $\kappa/2\pi = 44$ MHz, is much larger than the bare qubit linewidth $\gamma/2\pi < 2$ MHz. **b**, Extracted linewidths from the data in **a** (blue dots) are compared with theoretical values (red lines). As the qubit and cavity peaks approach degeneracy, the qubit peak becomes broader owing to spontaneous emission to the cavity mode, while the cavity decay is suppressed. Extra dephasing present only at low frequencies (the right side of the graph) causes a non-lorentzian line shape and excessive width. Measurements of the relaxation rate in the time domain (open blue circles) agree with theoretical estimates. Discrepancies arise due to flux noise and variations in non-radiative decay with frequency. The operating point for Figs 3–5 is $\Phi/\Phi_0 = 0.366$.

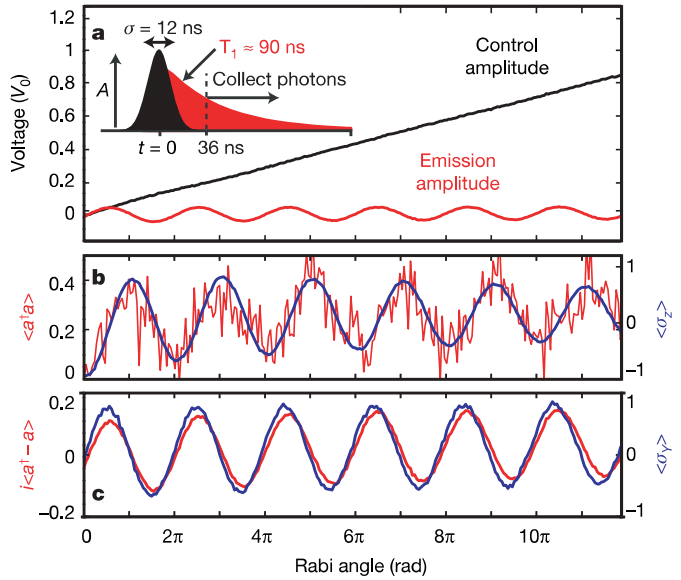

Figure 3 | Output of a single-photon source. Measurements of the qubit state are shown in blue, photon emission in red, and control signal in black. **a**, Measured drive (at $t = 0$ ns) and spontaneous emission voltage (at $t = 36$ ns) of cavity output, in units of zero-point voltage fluctuations $V_0 \approx 2\,\mu$V. The inset shows the time sequence, with a gaussian pulse at the qubit frequency and subsequent photon emission with relaxation time T_1. When the amplitude A of the drive rotating the qubit is linearly increased, the amplitude of the output voltage of the cavity is oscillatory. **b**, Photon number output of the cavity $\langle a^{\dagger}a\rangle$ (integrated from $t = 36$ ns to $t = 236$ ns) detected with a diode (left axis), and the measured qubit state $\langle\sigma_z\rangle$ (right axis). These peak when the qubit is in the excited state, after a π pulse; the agreement between qubit and photon states verifies the photon generation occurs as expected. After a π pulse, the integrated power is 38% of that expected for a single photon, setting the scale for the photon axis. Fits to the qubit decays are used to extrapolate the qubit polarization immediately after the control pulse, and are used to set the scale of the qubit axis. **c**, Integrated voltage of the output photons $i\langle a^{\dagger} - a\rangle$ (from $t = 36$ ns to t = 104 ns) compared with the qubit state $\langle\sigma_y\rangle$, measured with a Ramsey experiment. The agreement shows that the phase of superposition states is also transferred from qubit to photon. Only 12% of the voltage for the $\pi/2$ superposition is collected here, owing to non-radiative decay and qubit dephasing, setting the scale of the voltage axis. The qubit amplitude is again extrapolated to the time immediately following the control pulse.

Using markovian master equation simulations, the complete time dynamics can be predicted with excellent accuracy, as shown for the homodyne voltage in Fig. 4. Several features of the time dynamics are striking. First, because the control pulse sets the rotation axis, and the qubit state sets the emission phase, the control and generated photons are orthogonal in phase, which allows the two signals to be completely separated in homodyne detection. In the generated photon quadrature, rapid time oscillations are apparent during the control pulse; this is a direct observation of the Rabi oscillation of the qubit through its spontaneous emission. After the pulse, the qubit emits with a phase that depends on its final state, resulting in oscillations in the control amplitude that smoothly connect to the time oscillations. Finally, there is a very-low-frequency oscillation in time. Photons are emitted at the qubit frequency, which is slightly detuned from the drive frequency. The result is a beating, with a half-period shown in both theory and data images, indicative of a frequency separation between the input and output photons in addition to the phase and time separations.

These simulations can also be used to calibrate the efficiency of the source. They are based on independently measured parameters of the system, with the only unknown parameter being the overall amplitude scaling. However, this scaling parameter is the same for both the measured control and measured emission photons. Therefore, comparison of the amplitude of the control pulse in theory and experiment yields a calibration for the single-photon emission, which allows a calculation of the efficiency of the sources.

Two metrics of efficiency characterize the performance of the system. The source efficiency is the fraction of time in which a photon is emitted after a control pulse. This depends on the final polarization of the qubit and the ratio of radiative to non-radiative channels. In generating a single photon, the π-pulse leaves the qubit 87% polarized, and nearly all decay is radiative ($\gamma_\kappa/\gamma > 90\%$), giving source efficiency of more than 78%. For generating a superposition of zero and one photon, the quadrature phase of the photon must also be controlled. Here, the qubit is 77% polarized along σ_y, but a dephasing rate $\gamma_\phi \approx 1$ MHz leads to only $\gamma_\kappa/(\gamma + 2\gamma_\phi) = 50\%$ radiation efficiency, giving a total source efficiency of 39%.

A second metric, the usable source efficiency, is somewhat lower in the current experiment, because the control pulse is slow and a delay is necessary to reject any control photons which could give a double-photon event. In the data of Fig. 3, collection of radiation begins after

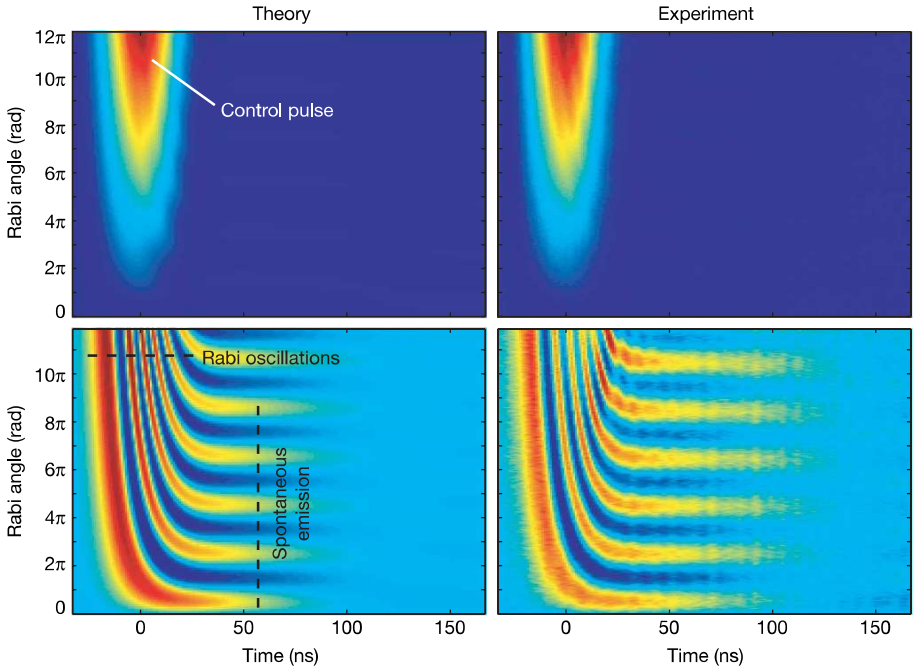

Figure 4 | Direct observation of the free induction decay of a superconducting qubit. Theoretical predictions (left) for both quadratures of the homodyne voltage, both in-phase (top) and out-of-phase (bottom) with the drive, agree well with experimental measurements of the two phases (right). Because emission is always orthogonal to the rotation axis, the spontaneous emission and control signal are phase separable. The homodyne sine waves in Fig. 3c are calculated as integrals of horizontal slices through this data at different angles. The frequency of these oscillations, coupled with a gain known from measurements of the control pulse, provide a calibration, which is used to predict the experimental emission data. The qubit and drive are slightly detuned by a fluctuating amount due to flux instability (of the order of 3 MHz), so there is a slow beat note in the time direction. This fluctuating detuning is modelled by adding the predicted homodyne emission at two detunings, ± 1.5 MHz. The fast oscillations in the time domain are a direct measure of the Rabi oscillations of the qubit.

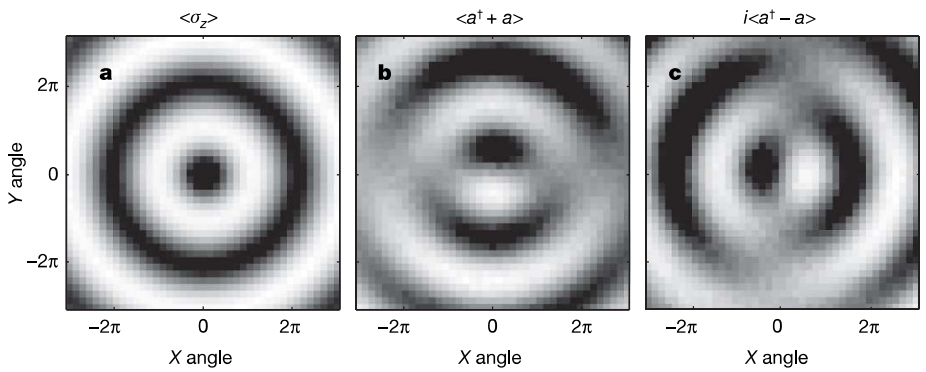

Figure 5 | Mapping the qubit state onto the photon state. a, Measurement of the qubit state $\langle\sigma_z\rangle$ after rotations by pulses of arbitrary amplitude and phase. Regardless of the phase of the pulse, the qubit oscillates to a peak after a π pulse. **b**, **c**, Fluorescence tomography. The amplitude of the voltage measured in each homodyne quadrature, $\langle a + a^{\dagger}\rangle$ and $i\langle a^{\dagger} - a\rangle$, agree with expectations for $\langle\sigma_x\rangle$ and $\langle\sigma_y\rangle$. Oscillations around the *x*-axis produce a signal in $i\langle a^{\dagger} - a\rangle$ and none in $\langle a + a^{\dagger}\rangle$. This shows the ability to map an arbitrary qubit state onto a photon state, as well as the ability to characterize a qubit state through spontaneous emission.

three standard deviations of the control pulse gaussian, making the likelihood of contamination by a control photon less than 0.01%. Integrating the measured spontaneous emission, the number of detected photons is measured directly, yielding an efficiency of 38% for the single-photon source, and 12% for the homodyne voltage of the superposition state, which is again lower, owing to dephasing. Even rejecting the emission contaminated by control pulse photons, which contains the high signal-to-noise part of the emission, a substantial fraction of one photon is recovered. If a less stringent rejection threshold of 1% is chosen, efficiencies rise to 46% for power and 16% for homodyne voltage. In future experiments, this could be improved further with faster pulses, longer coherence times, or fast tunability of the qubit frequency, achieving usable source efficiencies close to 100%.

Tomography presents an even more powerful tool for characterizing the transfer from qubit state[26] to photon state[27,28] (Fig. 5). Here, qubit tomography is performed by applying control pulses of arbitrary phase and amplitude, and performing a dispersive measurement[25] of the qubit state $\langle\sigma_z\rangle$. This yields the expected concentric rings for a qubit initially in the ground state (Fig. 5a). Similarly, for the same set of control pulses, both quadratures of the output homodyne voltage are recorded (Fig. 5b, c). These show excellent agreement with the expected σ_x and σ_y components of the qubit state[26]. This fluorescence tomography technique allows a full characterization of the qubit by looking at the spontaneous emission at the output, directly observing a superconducting qubit at its Larmor frequency. Moreover, this means that a qubit state at arbitrary points on the Bloch sphere can be transferred onto a photon state, thus moving information from a stationary qubit to a "flying qubit", one of the DiVincenzo resources for quantum information processing[29].

The mapping of qubit states onto photon states allows for the use of microwave photons as a true resource for quantum information on a chip. These photons are generated on-demand with a high repetition rate, good spectral purity, and high efficiency. This is a convenient means of creating non-classical states of light to interact with atoms, in which the photon can be guided along the wires of an integrated circuit, allowing them to be shuttled around a chip. The generation of single photons, and superpositions of photon states, is an important step towards on-chip quantum optics experiments.

Received 6 February; accepted 24 July 2007.

1. Schuster, D. I. *et al.* Resolving photon number states in a superconducting circuit. *Nature* **445**, 515–518 (2007).
2. Oxborrow, M. & Sinclair, A. Single-photon sources. *Contemp. Phys.* **46**, 173–206 (2005).
3. Clauser, J. F. Experimental distinction between the quantum and classical field-theoretic predictions for the photoelectric effect. *Phys. Rev. D* **9**, 853–860 (1974).
4. Kimble, H. J., Dagenais, M. & Mandel, L. Photon antibunching in resonance fluorescence. *Phys. Rev. Lett.* **39**, 691–695 (1977).
5. Diedrich, F. & Walther, H. Nonclassical radiation of a single stored ion. *Phys. Rev. Lett.* **58**, 203–206 (1987).
6. Basche, T., Moerner, W. E., Orrit, M. & Talon, H. Photon antibunching in the fluorescence of a single dye molecule trapped in a solid. *Phys. Rev. Lett.* **69**, 1516–1519 (1992).
7. Brunel, C., Lounis, B., Tamarat, P. & Orrit, M. Triggered source of single photons based on controlled single molecule fluorescence. *Phys. Rev. Lett.* **83**, 2722–2725 (1999).
8. Lounis, B. & Moerner, W. E. Single photons on demand from a single molecule at room temperature. *Nature* **407**, 491–493 (2000).
9. Kurtsiefer, C., Mayer, S., Zarda, P. & Weinfurter, H. Stable solid-state source of single photons. *Phys. Rev. Lett.* **85**, 290–293 (2000).
10. Michler, P. *et al.* Quantum correlation among photons from a single quantum dot at room temperature. *Nature* **406**, 968–970 (2000).
11. Darquie, B. *et al.* Controlled single-photon emission from a single trapped two-level atom. *Science* **309**, 454–456 (2005).
12. Maitre, X. *et al.* Quantum memory with a single photon in a cavity. *Phys. Rev. Lett.* **79**, 769–772 (1997).
13. Brattke, S., Varcoe, B. T. H. & Walther, H. Generation of photon number states on demand via cavity quantum electrodynamics. *Phys. Rev. Lett.* **86**, 3534–3537 (2001).
14. Moreau, E. *et al.* Single-mode solid-state single photon source based on isolated quantum dots in pillar microcavities. *Appl. Phys. Lett.* **79**, 2865–2867 (2001).
15. Santori, C., Fattal, D., Vuckovic, J., Solomon, G. S. & Yamamoto, Y. Indistinguishable photons from a single-photon device. *Nature* **419**, 594–597 (2002).
16. Pelton, M. *et al.* Efficient source of single photons: A single quantum dot in a micropost microcavity. *Phys. Rev. Lett.* **89**, 233602 (2002).
17. Kuhn, A., Hennrich, M. & Rempe, G. Deterministic single-photon source for distributed quantum networking. *Phys. Rev. Lett.* **89**, 067901 (2002).
18. McKeever, J. *et al.* Deterministic generation of single photons from one atom trapped in a cavity. *Science* **303**, 1992–1994 (2004).
19. Keller, M., Lange, B., Hayasaka, K., Lange, W. & Walther, H. Continuous generation of single photons with controlled waveform in an ion-trap cavity system. *Nature* **431**, 1075–1078 (2004).
20. Blais, A., Huang, R.-S., Wallraff, A., Girvin, S. M. & Schoelkopf, R. J. Cavity quantum electrodynamics for superconducting electrical circuits: An architecture for quantum computation. *Phys. Rev. A.* **69**, 062320 (2004).
21. Purcell, E. M. Spontaneous emission probabilities at radio frequencies. *Phys. Rev.* **69**, 681 (1946).
22. Koch, J. *et al.* Charge insensitive qubit design derived from the Cooper pair box. *Phys. Rev. A* (in the press); preprint at ⟨http://arxiv.org/cond-mat/0703002⟩ (2007).
23. Bouchiat, V., Vion, D., Joyez, P., Esteve, D. & Devoret, M. H. Quantum coherence with a single cooper pair. *Phys. Scr.* **T76**, 165–170 (1998).
24. Wallraff, A. *et al.* Strong coupling of a single photon to a superconducting qubit using circuit quantum electrodynamics. *Nature* **431**, 162–167 (2004).
25. Wallraff, A. *et al.* Approaching unit visibility for control of a superconducting qubit with dispersive readout. *Phys. Rev. Lett.* **95**, 060501–060504 (2005).
26. Steffen, M. *et al.* State tomography of capacitively shunted phase qubits with high fidelity. *Phys. Rev. Lett.* **97**, 050502 (2006).
27. Smithey, D. T., Beck, M., Raymer, M. G. & Faridani, A. Measurement of the Wigner distribution and the density matrix of a light mode using optical homodyne tomography: application to squeezed states and the vacuum. *Phys. Rev. Lett.* **70**, 1244–1247 (1993).
28. Leonhardt, U. *Measuring the Quantum State of Light* (Cambridge Univ. Press, 1997).
29. DiVincenzo, D. P. The physical implementation of quantum computation *Fortschr. Phys.* **48**, 771–783 (2000).

Acknowledgements This work was supported in part by the National Security Agency under the Army Research Office, the NSF, and Yale University. A.A.H. acknowledges support from Yale University via a Quantum Information and Mesoscopic Physics Fellowship.

Author Information Reprints and permissions information is available at www.nature.com/reprints. The authors declare no competing financial interests. Correspondence and requests for materials should be addressed to R.J.S. (robert.schoelkopf@yale.edu).